Synthesis, DNA/RNA-interaction and biological activity of benzo[*k,l*]xanthene lignans

Lidija Marija Tumir,[a] Iva Zonjić,[a] Kristina Žuna,[b] Sandra Radić Brkanac,[c] Marijana Jukić,[e] Ana Huđek,[b] Ksenija Durgo,[b] Ivo Crnolatac,[a] Ljubica Glavaš-Obrovac,[e] Nunzio Cardullo,[d] Luana Pulvirenti,[d] Vera Muccilli,[d] Corrado Tringali,[d] Marijana Radić Stojković[a*]

[a] Ruđer Bošković Institute, Division of Organic Chemistry and Biochemistry, Bijenička cesta 54, 10000 Zagreb, Croatia

[b] Faculty of Food Technology and Biotechnology, University of Zagreb, Pierrotijeva 6, 10000 Zagreb, Croatia

[c] University of Zagreb, Faculty of Science, Department of Biology, Rooseveltov trg 6/III, HR-10 000, Zagreb, Croatia

[d] Dipartimento di Scienze Chimiche, Università degli Studi di Catania, Viale A. Doria 6, I-95125 Catania, Italy.

[e] Department of Medicinal Chemistry, Biochemistry and Laboratory Medicine, Faculty of Medicine Osijek, Josip Juraj Strossmayer University of Osijek, Huttlerova 4, HR-31000 Osijek, Croatia

*Corresponding author: Marijana Radić Stojković

Division of Organic Chemistry and Biochemistry, Ruđer Bošković Institute, P. O. Box 180, 10002 Zagreb, Croatia, E-mail: mradic@irb.hr, Phone: (+3851) 4571 220, Fax: (+3851) 46 80 195

Abstract

Interactions of two newly synthesized and six previously reported benzoxanthene lignans (BXLs), analogues of rare natural products, with DNA/RNA, G-quadruplex and HSA were evaluated by a set of spectrophotometric methods. Presence/absence of methoxy and hydroxy groups on the benzoxanthene core and minor modifications at C-1/C-2 side pendants – presence/absence of phenyl ring and presence/absence of methoxy and hydroxy groups on phenyl ring – influenced the binding strength to double-stranded (ds-) and G-quadruplex structures. In general, compounds without phenyl ring showed stronger fluorescence changes upon binding to ds-DNA/RNA while a derivative with butyl chain displayed DNA (GC-DNA) over RNA selectivity. On the other hand, BXLs with an unsubstituted phenyl ring showed the best stabilization effects of G-quadruplex. Circular dichroism spectroscopy results suggest mixed binding mode, groove binding and partial intercalation, to ds-DNA/RNA and end-stacking to top or bottom G-tetrads as the main binding modes of BXLs to those targets. All compounds exhibited micromolar binding affinities toward HSA and an increased protein thermal stability. Moderate to strong antiradical scavenging activity was observed for all BXLs with hydroxy groups at C-6, C-9 and C-10 positions of the benzoxanthene core, except for derivative bearing methoxy groups at these positions. BXLs with unsubstituted or low-substituted phenyl ring and one derivative without phenyl ring showed strong growth inhibition of Gram-positive *Staphylococcus aureus*. All compounds showed moderate to strong tumor cell growth-inhibitory activity and cytotoxicity.

Keywords: DNA/RNA recognition • benzo[*k,l*]xanthene lignans • G-quadruplex interaction • HSA interaction • antiproliferative effect

1. Introduction

Dimeric lignans and neolignans are plant secondary metabolites of the phenylpropanoid family with interesting biological activities including antioxidant, antitumor, anti-inflammatory, antiangiogenic, cardiovascular, antiviral and antimicrobial.[1-6] In addition, they represent a valuable source of building blocks exploitable in the field of organic and medicinal chemistry. Well-known members of the lignan family, podophyllotoxin and its derivatives, etoposide and teniposide are used for treating genital warts and as a form of chemotherapy for several cancers, administered alone or in combination with other antitumor drugs.[7, 8] Rufescidride, mongolicumin A and yunnaneic acid H (Figure 1) are a few examples of natural products reported in the literature that belong to benzo[*k,l*]xanthene lignans.[7, 9] Biological activity of this group of compounds has not been extensively studied to date due to a lack of effective synthetic methods and low availability in nature.[10, 11] Nevertheless, a biomimetic procedure for obtaining bioinspired benzo[*k,l*]xanthenes (BXLs), proposed by Tringali's group, stands out among some other examples in the literature for its good to high product yields.[12-14] These synthetic lignans, obtained by oxidative coupling of caffeic esters, have been tested for antioxidative, antiangiogenic, antimycotic, anti-inflammatory and antiproliferative properties.[15-20] But, so far their antibacterial effects have never been thoroughly examined.

The golden age of antibiotics, which revealed the majority of antibiotics still in use today, ended because the number of newly discovered compounds could not keep up with the increasing number of pathogenic bacterial strains, especially Gram-negative.[21] Consequently, many compounds isolated from plants or modeled upon natural compounds, including lignans, are being investigated today as potential antimicrobial agents.[22]

Due to their crucial roles in biological replication and protein synthesis, DNA and RNA are attractive targets for many classes of drugs. Insertion of planar (hetero)-cyclic aromatic chromophores between adjacent basepairs – intercalation, binding inside grooves and external binding are the most common drug interactions with DNA and RNA.[23]

Further, to enlighten the potential basis of their biological activity, several BXLs were screened for DNA interactions. STD-NMR experiments and molecular docking showed that benzoxanthenes intercalate into DNA with their planar core while the flexible pendants in C-1 and C-2 position bind along the minor groove.[13, 14] The study was carried out with the alternating polynucleotide poly(dGdC)$_2$ as a binding model. Poly(dGdC)$_2$ represents a classical B-helix with an amino group of guanine projecting in the minor groove and partially blocking the binding of small molecules. Thus, to get a better insight into BXLs interactions to nucleic acid structures (recognition of polynucleotide shape and/or bases), we introduced other DNA models such as ctDNA, a natural polynucleotide with a mixed base-pair composition (42% GC base pairs and 58% AT base pairs) and alternating AT polynucleotide, poly(dAdT)$_2$. For RNA model and as a representative of A-helix, we have chosen poly A – poly U, characterized by the major groove with a potential of binding of proteins and sterically demanding small molecules.[24, 25] Binding with G-quadruplex, based on Hoogsteen paired planar guanine ring-systems, was also studied since BXLs possess structural features (aromatic core and side-chains) required for the stabilization of quadruplexes.

Thus, one of our intents in this study was to investigate interactions of BXLs with an array of DNA (including G-quadruplex) and RNA by a set of spectrophotometric methods – UV/Vis, circular dichroism (CD) and fluorescence. The study included four BXLs (Scheme 1, CT-A1, CT-A2, CT-A4, CT-A14), previously studied with STD-NMR and molecular docking [13, 14] and four analogues of **CT-A2** (two of them newly synthesized) which, among studied benzo[*k,l*]xanthenes, displayed the most prominent antiproliferative activity and the highest predicted binding affinity toward poly(dGdC)$_2$ (Figure 1).[13, 17] **CT-A2** analogues (**CT-A19**, **CT-A22**, **CT-A23** and **CT-A24**) differed either in pendant alkyl linkers (methyl or ethyl) in positions 1 and 2 and/or in the presence of methoxy and/or hydroxy groups on the phenyl ring (Scheme 1). The introduction of such groups on the phenyl ring in CT-A2 analogues, could result in greater binding ability inside the groove (hydrophobic interactions and

displacement of solvent, favorable van der Waals interactions, as well as additional H-bonds with the bases). Modification in the linker length can give information about the impact of the linker flexibility on the strength of noncovalent interactions. [26]

In addition to DNA and RNA, we examined interactions of BXLs with the most predominant proteins in blood plasma, human serum albumin (HSA).

Our second goal was to investigate the antiradical, antiproliferative and antibacterial activity of BXLs since their close lead compound rufescidride, showed promising antibacterial activity.[27]

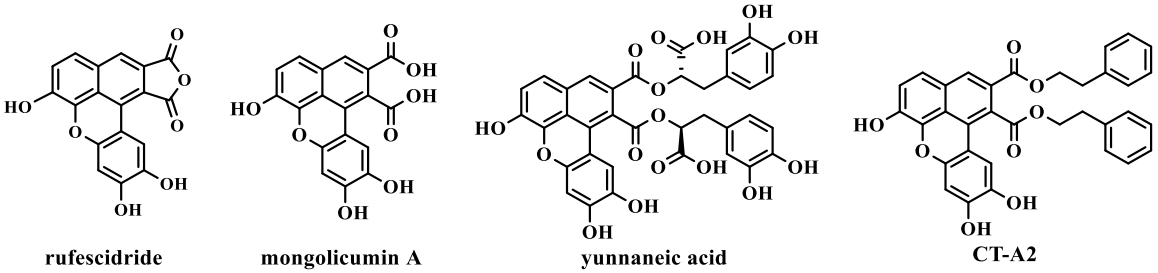

Figure 1. Chemical structures of natural benzo[*k,l*]xanthenes, rufescidride, mongolicumin A, yunnaneic acid H and synthetic benzo[*k,l*]xanthene **CT-A2**.

2. Results and discussion

2.1 Synthesis and characterization of compounds in the aqueous medium

The synthesis of benzo[*k,l*]xanthene lignans (to the follow benzoxanthenes simply or BXLs) has been carried out as previously reported by some of us.[13, 14, 18] As summarized in Scheme 1, these compounds are obtained by oxidative coupling of suitable caffeic esters (**2a**-**g**) in good yield. Compound **CT-A14** has been obtained by methylation of **CT-A1**. The structures of the newly synthesized benzoxanthenes **CT-A23** and **CT-A24** were determined by analysis of their MS, ^{1}H and ^{13}C NMR spectra, and corroborated by two-dimensional NMR experiments (HSQC and HMBC).

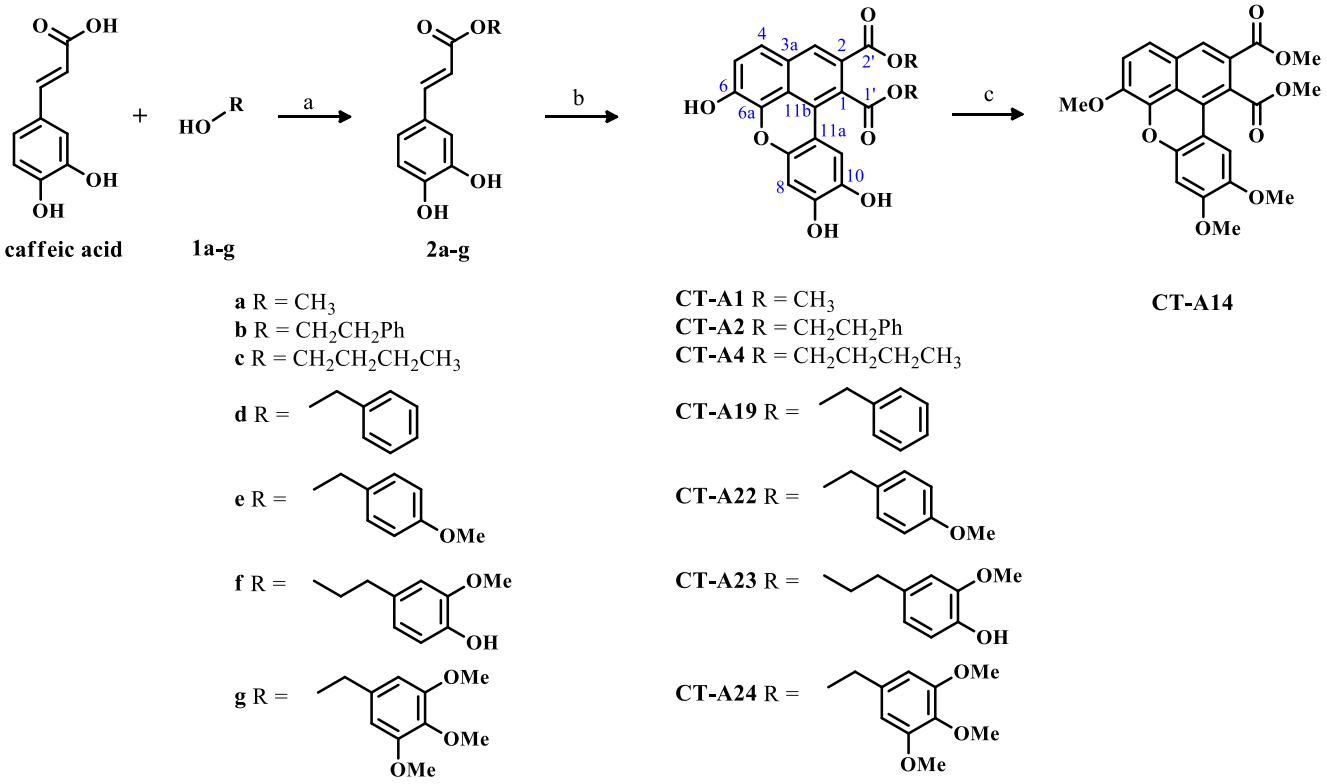

Scheme 1. Synthesis of benzoxanthene lignans. **a**) H_2SO_4, alcohol, reflux, 12 h (compounds **2a** and **2c**), DCC, alcohol, dry THF, 70 °C, 7 h (compounds **2d**-**g**); **b**) $Mn(OAc)_3$, $CHCl_3$, rt, 3 h; **c**) **CT**-**A1**, K_2CO_3, MeI, dry acetone, 56 °C, 12 h.

Solubility and UV/Vis characterization of BXLs were examined before DNA/RNA binding study. Benzoxanthenes were soluble in DMSO (up to $c = 5 \times 10^{-3}$ mol dm^{-3}). DMSO stock solutions of BXLs were stable during a few weeks in the dark/refrigerator. All measurements were recorded in Na-cacodylate buffer ($I = 0.05$ M for DNA/RNA/HSA measurements or $I = 0.1$ M for G-quadruplex) at pH 7. The volume ratio of DMSO was up to 1% for thermal melting experiments (ΔT_m) and CD titrations and 0.5‰ for fluorimetric titrations. Absorbancies of aqueous solutions of BXLs were proportional to their concentrations up to concentrations $c = 3 \times 10^{-5}$ mol dm^{-3} (Supporting information, SI) suggesting that studied compounds do not aggregate by intermolecular stacking at experimental conditions used. Absorption maxima and corresponding molar extinction coefficients (ε) are given in Table S1 (SI). Excitation spectra of BXLs were in acceptable agreement with their UV/Vis spectra (see spectra in SI).

2.2. Binding study of BXLs with double-stranded (ds-) DNA/RNA

Binding of BXLs to DNA and RNA polynucleotides (at the excess of a polynucleotide) was monitored with the fluorescence spectroscopy. Among ds-polynucleotides, we chose *calf thymus* DNA (ctDNA, 58% AT and 42% GC) and poly A – poly U (RNA), as models for a classical B-helix and characteristic A-helical structure, respectively.[28] After acquiring preliminary results with these polynucleotides, we selected those compounds exhibiting sufficient fluorescence changes with ctDNA and significant binding activity to perform additional experiments with synthetic DNA polynucleotides, poly(dAdT)$_2$ and poly(dGdC)$_2$.[25]

In some titration experiments, the fluorescence of BXLs was quenched by the addition of ds-polynucleotide, which was accompanied by a hypsochromic (blue) shift of emission maximum (2-30 nm). On the contrary, the polynucleotide addition to the aqueous buffer solution of **CT-A1** and **CT-A2** increased the fluorescence (SI). The fluorescence changes of the majority of benzoxanthenes with studied polynucleotides were not dependent on the structure of polynucleotide added. Exceptions to that were **CT-A22** and **CT-A24** where the increase and decrease of their fluorescence were observed on their addition to ctDNA and poly A-poly U solutions, respectively (SI). In almost all titrations with ds-polynucleotides, the fluorescence changes of **CT-A4** were too small for the accurate calculation of binding constants. Similar small changes were noticed in titrations of **CT-A19, CT-A22, CT-A23** and **CT-A24** with ctDNA and **CT-A19** with poly A – poly U. It was noted that **CT-A1** and **CT-A14** which differ only in one type of substituent (-OH vs $-OCH_3$) attached on C-6, C-9 and C-10 positions of benzoxanthene ring, caused opposite fluorimetric changes upon interaction with polynucleotides. While **CT-A1** caused the increase of fluorescence in the presence of DNA/RNA, **CT-A14** (SI) caused a decrease which probably can be ascribed to electron-donor properties of methoxy groups.

The binding constants *Ks* and ratios $n_{[\text{bound compound}]/[\text{DNA/RNA}]}$ obtained by processing of fluorimetric titration data with the Scatchard equation [29, 30] are summarized in Table 1. All studied compounds showed similar binding affinities toward ds-polynucleotides. Only **CT-A2** and **CT-A4** showed preferable binding to DNA, especially **CT-A4** that showed significant changes only upon the addition of GC-DNA (Figure 2). **CT-A2** analogues, **CT-A22** and **CT-A24** showed sufficient emission changes and hence binding activity only toward RNA (poly A – poly U) while **CT-A19** displayed such changes toward ctDNA.

Table 1. Binding constants ($\log K_s$)[a] and ratios *n*[b] ([bound compound]/ [polynucleotide phosphate]) calculated from the fluorescence titrations of BXLs with ds- polynucleotides at pH = 7.0 (buffer sodium cacodylate, I = 0.05 mol dm^{-3}).

	ctDNA			poly A - poly U			$p(dAdT)_2$			$p(dGdC)_2$		
	$\log K_s$	*n*	I/I_0[c]	$\log K_s$	*n*	I/I_0[c]	$\log K_s$	*n*	I/I_0[c]	$\log K_s$	*n*	I/I_0[c]
CT-A1	6.0	< 0.1	2.2	5.9	< 0.1	1.6	5.9	< 0.1	2.5	5.2	< 0.1	2.0
CT-A2	5.0	0.1	2.4	-[d]	-[d]	-[d]	5.3	< 0.1	1.9	5.1	< 0.1	1.9
CT-A4	-[d]	-[d]	-[d]	-[d]	-[d]	-[d]	-[d]	-[d]	-[d]	6.0	0.6	0.2
CT-A14	6.4	0.2	0.6	5.2	0.2	0.3	6.3	0.3	0.75	5.6	0.5	0.6
CT-A19	5.8	0.25[b]	0.7	-[d]	-[d]	-[d]				-[e]		
CT-A22	-[d]	-[d]	-[d]	5.2	0.25[b]	0.8				-[e]		
CT-A23	-[d]	-[d]	-[d]	-[d]	-[d]	-[d]				-[e]		
CT-A24	-[d]	-[d]	-[d]	5.6	0.25[b]	0.5				-[e]		

[a] Correlation coefficients were >0.99 for most calculated K_a.

[b] Processing of titration data using Scatchard equation[29] gave values of ratio *n*[bound compound]/[polynucleotide except in titrations with **CT-A19**, **CT-A22** and **CT-A24** with poly A – poly U or ctDNA where ratio *n* had to be fixed to 0.25

[c] I_0 – starting fluorescence intensity of BXL; I – fluorescence intensity of BXL /polynucleotide complex calculated by Scatchard equation.[29]

[d] small /linear fluorescence change / no fluorescence change / high divergences of fluorescence intensities disabled calculation of stability constant

[e] not determined

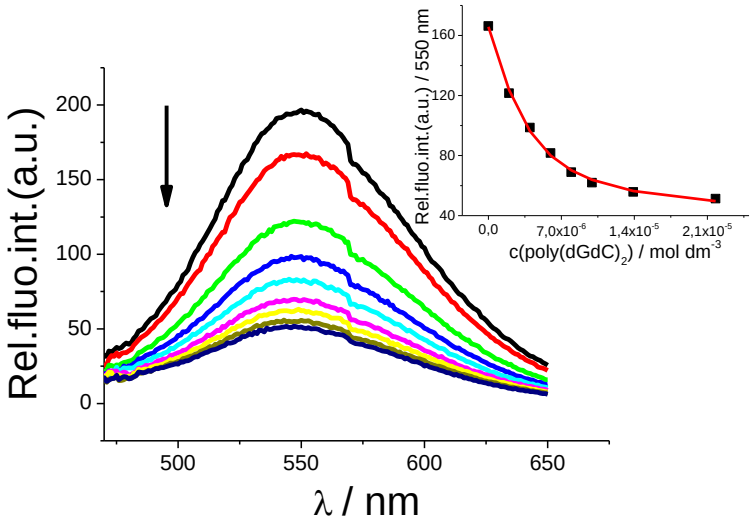

Figure 2. Changes in fluorescence spectrum of **CT-A4** (c= 2.0 × 10^{-6} mol dm^{-3}, λ_{exc}=398 nm) upon titration with poly(dGdC)$_2$ (c= 2 × 10^{-6} –2.2 × 10^{-5} mol dm^{-3}); Inset: Dependence of **CT-A4** fluorescence at λ_{max} = 550 nm on c(poly(dGdC)$_2$), at pH=7, sodium cacodylate buffer, I = 0.05 mol dm^{-3}.

Usually, non-covalent binding of small molecules to ds-polynucleotides affects the thermal stability of helices, thus giving different melting temperature (T_m) values. ΔT_m value is the difference between the T_m value of free polynucleotide and that obtained in a complex with a small molecule.[31]

Almost all benzoxanthenes showed a small stabilization effect (≤ 1°C) of mixed DNA base pairs (ctDNA composition, 58% AT, 42% GC), among them, only **CT-A1** and **CT-A14** stabilize AT-DNA (SI, Table S2). None of the studied compounds showed any stabilization effect of AU basepairs except **CT-A14** (ΔT_m = +0.9°C).

CD spectroscopy is a sensitive technique for monitoring DNA conformational changes resulting from small molecule binding.[32] Additional information on the small molecule-polynucleotide complexes can be acquired via an induced CD (ICD) signal of achiral small molecules when they form complexes with ds-polynucleotides.[33, 34] Further since polynucleotides do not absorb in the area above 300 nm while compounds display the UV/Vis spectra until 600 nm, the most reliable information on compounds' interaction with polynucleotides can be obtained in this area (Figure 3, SI).

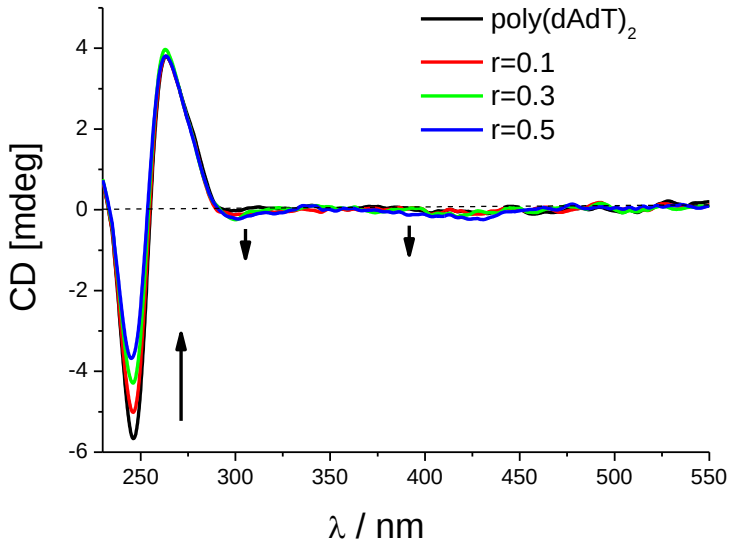

Figure 3. CD titration of poly(dAdT)$_2$ (c = 3.0 × 10^{-5} mol dm^{-3}) with **CT-A1** at molar ratios ***r*** = [compound] / [polynucleotide] (pH = 7.0, buffer sodium cacodylate, I = 0.05 mol dm^{-3}).

The addition of the majority of benzoxanthenes resulted in a small decrease in CD spectra of DNA and RNA polynucleotides (Figure 3, SI). Weak negative induced CD (ICD) signals located around 300 nm were mainly visible in titrations with DNA polynucleotides, only in few cases with poly A – poly U. Some compounds like **CT-A1** and **CT-A4** showed additional weak negative ICD signals around 400 nm with poly(dAdT)$_2$ and poly(dGdC)$_2$, respectively. Unlike other compounds, **CT-A2** showed a significant increase of CD spectra of GC-DNA. Additionally, a clear isodichroic point observed for **CT-A1** and AT-DNA strongly suggests one dominant interaction mode of this compound with the DNA chiral axis (Figure 3, SI).[34]

Weak negative ICD sign, resulting from the "parallel" orientation of the long axis of ligand to the long axis of adjacent base-pairs is a strong indication of intercalative binding.[32, 33, 35] Such changes can also be indicative of a groove binding.[34] This is additionally supported by the negligible thermal stabilization of ds-polynucleotides, which is not characteristic for the classical intercalation. Despite the strong binding indicated by fluorescence spectroscopy, some complexes like **CT-A1** or **CT-A14** with poly A – poly U, produced negligible ICD intensities. Such changes are most probably a result of partial intercalation and/or groove binding where the long axis of the aromatic core is positioned at some angle to the long axis of adjoining basepairs resulting in the abolishment of positive and negative contribution.[35]

Observed mixed binding mode (groove binding, partial intercalation) of benzoxanthenes suggested by CD spectroscopy agrees nicely with results of DF-STD analysis obtained for **CT-A1**, **CT-A2**, and **CT-A4**.[13, 14] BMI (binding mode indexes) values, calculated on the base of the relative intensities of STD effects, indicated intercalation of the planar benzoxanthene core between the base pairs of the GC-DNA. Also, subsidiary BMI' values referring to the chemical appendages in positions C-1 and C-2 of the benzoxanthene core implied another mode of binding, the interaction inside the groove. While BMI values in most cases straightforwardly point to one dominant mode of binding (intercalation or minor groove binding or external backbone binding), conclusions of additional binding mode supported solely on BMI' values can be more ambiguous.[36] Nevertheless, it is always recommendable to combine more methods for characterization of small molecule-DNA complexes, preferentially CD spectroscopy as a sensitive indicator of conformational changes of nucleic acid upon interaction with ligands. Thus, taking into account BMI'

values for **CT-A1**, **CT-A2** and **CT-A4**, structural features of studied benzoxanthenes and their CD/ICD signals, it may be concluded that BXLs form favourable interactions (van der Waals contacts, hydrogen bonds, hydrophobic interactions) inside the groove. The other possible binding mode is partial intercalation (stacking interactions) between adjacent base pairs. Compared to **CT-A2**, smaller emission changes and slightly weaker binding towards polynucleotides can be noticed with **CT-A2** analogues (**CT-A19**, **CT-A22**, **CT-A23** and **CT-A24**). Thus, either pendant alkyl linker in positions 1 and 2 (methyl linkers in **CT-A19**, **CT-A22** and **CT-A24**) or most probably the presence of methoxy and/or hydroxy groups on phenyl ring (**CT-A22**, **CT-A23** and **CT-A24**) affect the strength of noncovalent interactions.

2.3. Interaction of BXLs with G-quadruplex

Lots of studies support the involvement of G-quadruplex structures in important biological processes like as DNA replication, recombination, expression of some oncogenes, epigenetic regulation, maintenance of telomeres stability and telomerase inhibition in cancer cells.[37]

Except with alternating AT- and GC-DNA copolymers, the interaction of BXLs has been investigated with DNA quadruplex using oligonucleotide Tel22, which is frequently used as *in vitro* model for the formation of such structures in the human telomere.[38, 39] In Na^+ solutions intramolecularly folded Tel22 consists of three stacked G-tetrads connected by two lateral loops and a central diagonal loop.[40]

Interactions of BXLs with Tel 22 were studied by fluorimetric and CD titrations and thermal melting experiments.

Fluorescence spectra of BXLs changed (increase or quenching) upon the addition of G-quadruplex solution. The binding constants and stoichiometries of complexes were calculated for the concentration range corresponding to 20-80% complex formed using non-linear least-square program SPECFIT.[41] For all fluorimetric titrations, the best fit was obtained for 1:1 benzoxanthene – Tel22 stoichiometry (Table 2, Figure 4, SI). Compared to other analogues, the smallest affinities toward Tel22 showed **CT-A23** and **CT-A24** possessing a more substituted phenyl ring.

All studied BXLs, except **CT-A4**, showed the stabilization effect of Tel22 (Table 2). Regardless of the pendant alkyl linkers (methyl or ethyl linker on C-1 and C-2 pendants), the largest stabilizations of Tel22 exhibited **CT-A2** and **CT-A19** with unsubstituted phenyl ring (Figure 5). This stabilization effect can be explained by additional π-π stacking interactions. In the case of **CT-A23** and **CT-A24**, stacking interactions, arising from phenyl moieties, are probably weakened due to the steric hindrance of hydroxy/methoxy substituents on the phenyl ring. All compounds displayed negligible changes (small decrease) of CD spectra of Tel22 (Figure 5, SI). Taking into account the binding affinities and 1:1 benzoxanthene – Tel22 binding stoichiometry, stabilization effects of quadruplex structure and negligible changes of CD spectra of Tel22, it can be concluded that benzoxanthenes most likely bind via end-stacking π-π interactions with the top or bottom quartets of Tel22.[37, 42]

Table 2. Binding constants ($\log Ks$)[a] for 1:1 complexes of BXL-Tel22 and changes of fluorescence intensity I/I_0[b] calculated from the fluorescence titrations and ΔT_m[d] values (°C) of Tel22 upon addition of ratio[e] $\boldsymbol{r}$ = 0.3 of BXLs at pH = 7.0 (sodium cacodylate buffer, I = 0.1 mol dm^{-3}).

compound	logK_s	I/I_0[b]	ΔT_m / °C
CT-A1	4.37±0.04	3.3	1.2
CT-A2	5.13±0.04	5.1	14
CT-A4	>5[c]	<1[c]	0.1
CT-A14	5.86±0.04	0.2	2.3
CT-A19	4.26±0.16	5.4	8.8
CT-A22	5.64±0.07	0.8	3.3
CT-A23	4.03±0.10	13.9	1.8
CT-A24	<4[c]	>1[c]	2.1

[a] Stability constant Ks and stoichiometry calculated by processing the titration data SPECFIT program[41]

[b] Changes in fluorescence of BXLs induced by complex formation (I_0 was emission intensity of free compound and I_{lim} was emission intensity of a complex, calculated by processing the titration data SPECFIT program).[41]

[c] Small/linear fluorescence change disabled calculation/enabled only an estimation of stability constant

[d] Error in ΔT_m: ± 0.5 °C;

[e] ***r*** = [compound]/[polynucleotide]

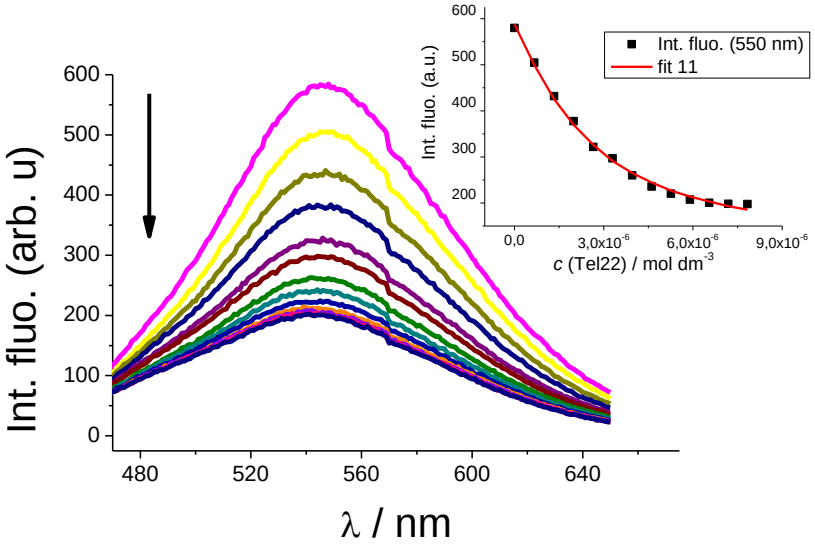

Figure 4. Changes in fluorescence spectrum of **CT-A14** (c= 2.0 × 10^{-6} mol dm^{-3}, λ_{exc}=394 nm) upon titration with Tel22 (c= 4.5 × 10^{-6} – 6.2 × 10^{-5} mol dm^{-3}); Inset: Experimental (■) and calculated (—) fluorescence intensities of **CT-A14** at λ_{em} = 550 nm upon addition of Tel22 (pH = 7.0, Na cacodylate buffer, I = 0.1 mol dm^{-3}).

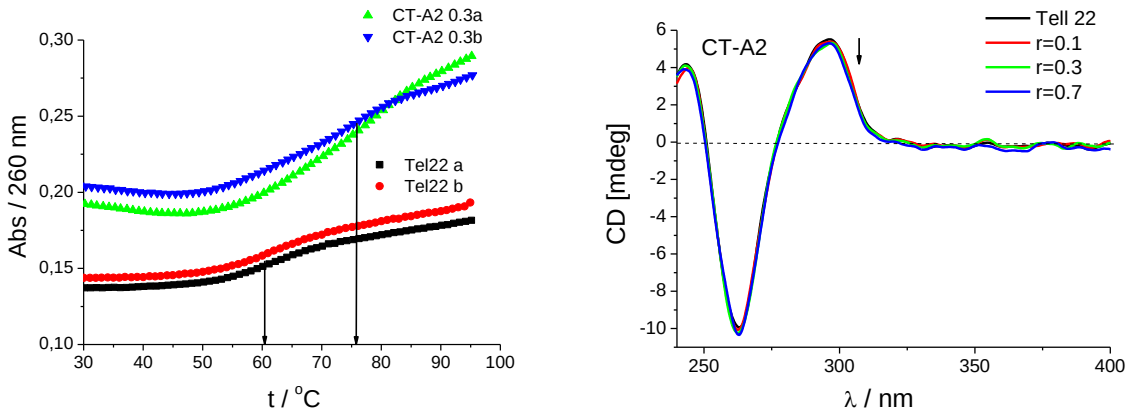

Figure 5. Left: Melting curves of Tel22 upon addition of **CT-A2**; c (Tel22) =1.4 ×10^{-6} M; ratio, ***r*** =[compound] / [oligonucleotide]=0.3. Right: CD titration of Tel22 (c = 3.0 × 10^{-5} mol dm^{-3}) with **CT-A2** at molar ratios ***r*** = [compound] / [polynucleotide] indicated in the graph legend (pH = 7.0, buffer sodium cacodylate, I = 0.1 mol dm^{-3}).

2.4. HSA binding study

HSA is a major plasma protein participating in binding and transfer of many different substances, including drugs.[43] Since binding to HSA affects the active concentration of drugs in cell compartments, it is beneficial to characterize the interaction of biologically active small molecules with this protein. Fluorescence spectroscopy and differential scanning calorimetry (DSC) have been used for the characterization of benzoxanthene–HSA complexes.

Titrations with human serum albumin yielded an emission increase of all studied BXLs (Figure 6, SI). BXLs showed rather high binding affinities toward HSA (Table 3). The greatest affinity among benzoxanthenes exhibited **CT-A4** and **CT-A22** while the weakest one was calculated for **CT-A14**. Despite the small difference on C-6, C-9 and C-10 positions of benzoxanthene core (–OH vs –OCH_3), the binding affinity of **CT-A1** was two orders of magnitude higher than of **CT-A14**. The number of binding sites on HSA calculated based on the Scatchard equation ranged from 1 to 4 (Table 3). **CT-A22** and **CT-A4** with the highest binding affinities have one and two binding sites on HSA, respectively. Two main drug binding sites are known from the literature as site 1 located in subdomain IIA and site 2 in subdomain IIIA.[44-47]. Nevertheless, the goal here was to evaluate binding affinities and the number of binding sites and not to determine the main binding site of benzoxanthenes and predict the accurate geometry of the benzoxanthene-HSA complex using *in silico* methods.[48]

Table 3. Binding constants (log*Ks*)[a] and ratios n[b] ([bound compound]/[HSA]) calculated from the fluorescence titrations of BXLs with HSA at pH = 7.0 (buffer sodium cacodylate, I = 0.05 mol dm^{-3}).

	HSA		
compound	logK_s	*n*	I/I_0[c]
CT-A1	6.6	3.9	2.3
CT-A2	5.8	3.9	3.7
CT-A4	7.5	2.1	2.2
CT-A14	4.7	3.9	2.1
CT-A19	6.5	3[d]	1.6
CT-A22	7.1	1.3	1.8
CT-A23	5.3	3[d]	4.6
CT-A24	6.8	3[d]	1.5

[a] Accuracy of *n* ± 10 - 30%, consequently log*Ks* values vary in the same order of magnitude;

[b] Processing of titration data using Scatchard equation gave values of ratio *n*[bound compound]/[polynucleotide];

[c] I_0 – starting fluorescence intensity of BXL; *I* – fluorescence intensity of BXL /HSA complex calculated by Scatchard equation.

[d] *n* ratio was fixed to 3

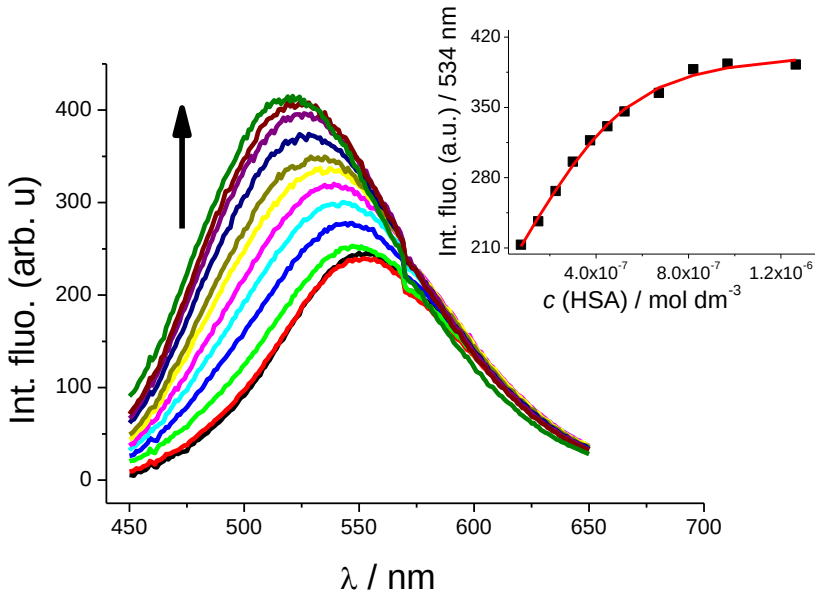

Figure 6. Changes in fluorescence spectrum of **CT-A1** (c= 2 × 10^{-6} mol dm^{-3}, λ_{exc}=393 nm) upon titration with HSA (c= 7.5 × 10^{-8} – 1.3 × 10^{-6} mol dm^{-3}); Inset: Dependence of **CT-A1** fluorescence at λ_{max} =534 nm on c(HSA), at pH=7,sodium cacodylate buffer, I=0.05 mol dm^{-3}.

The binding of a drug to protein causes changes in protein structure. Besides, the formation of the protein-small molecule complex is driven by enthalpic and entropic contributions, whose balance determines free Gibbs energy of interaction.[49] Thus, drug binding causes changes in the thermostability of protein that can be monitored by differential scanning calorimetry (DSC). Single HSA, as well as benzoxanthene – HSA complexes, showed broad, bimodal endothermic transitions connected with albumin denaturation.[50, 51] Two transitions were attributed to the first and the second denaturation temperature. The addition of different BXLs generally caused small change (positive or negative) of the first transition temperature, except for **CT-A14** while the changes of the second transition were more significant especially for **CT-A1**, **CT-A2**, **CT-A4** and **CT-A24** (SI, Table S3). These results are in accordance with the micromolar affinities for benzoxanthene – HSA complexes calculated from the fluorimetric titrations.

2.5. Antibacterial effects of BXLs

Preliminary studies of the antibacterial activity of benzoxanthene-related compounds have not shown significant results, except for rufescidride, which was isolated from plants *Cordia rufescens* and *Taraxum mongolicum*.[9, 14, 27] However, the studies with the compounds used in this work have not been thoroughly conducted to date.

The antibacterial effect was examined on Gram-positive (*Staphylococcus aureus*) and Gram-negative (*Escherichia coli* K-12 MG1655, *Salmonella enterica* serovar serotype Typhimurium LT21 and *Salmonella enterica* serotype Typhimurium TA100, a mutant strain with the damaged structure of cell wall) bacteria (Figure 7).

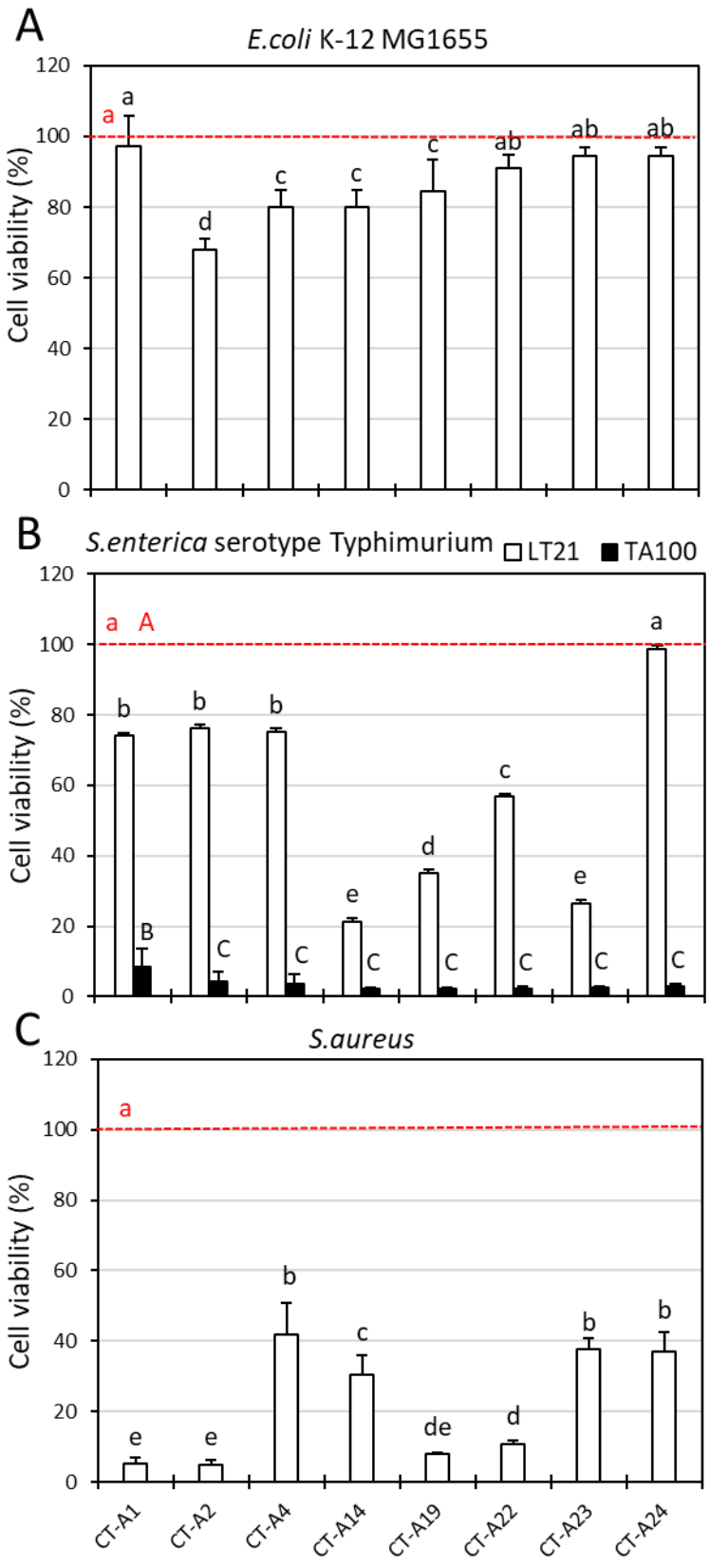
A
E.coli K-12 MG1655
Cell viability (%)
B
S.enterica serotype Typhimurium
LT21
TA100
Cell viability (%)
C
S.aureus
Cell viability (%)
CT-A1
CT-A2
CT-A4
CT-A14
CT-A19
CT-A22
CT-A23
CT-A24

Figure 7. The effect of BXLs on the viability of different G- (A, B) and G+ (C) bacteria. The viability was determined after a 1 h exposure period to 50 µM of BXLs or negative control (red dotted line). Standard deviations are presented by error bars. Different letters indicate significantly different values at $P < 0.05$ according to ANOVA.

The cytotoxic effect of benzoxanthenes was evaluated by one-hour incubation of bacterial strains and tested compounds, before seeding to the plates. The concentration of BXLs was 5×10^{-6} M. After incubation at 37 °C for 24 h, the number of grown bacterial colonies was counted and the survival was expressed as a percentage (compared to the negative control). The majority of studied benzoxanthenes showed weak inhibitory effects on *Escherichia coli* K-12 MG1655 growth (Figure 7A). Only **CT-A2** showed a small effect, with the inhibition of bacteria growth of 30%. On the other hand, **CT-A14** and **CT-A23** showed significant cytotoxic effect (growth inhibition ≤ 70%) against another Gram-negative bacteria, *S. enterica* Typhimurium LT21 (Figure 7B).[52, 53] Even **CT-A19** and **CT-A22** showed a moderate inhibitory effect on that bacterial strain. Thus, almost all **CT-A2** analogues were active except **CT-A24** and their parent compound **CT-A2**. Interestingly, **CT-A14** with methoxy groups on C-6, C-9 and C-10 positions of benzoxanthene core was, beside **CT-A23**, the most active while **CT-A24** had no activity. Obviously, the presence of methoxy groups on benzoxanthene core or methyl linkers in positions 1 and 2 act favorably on growth inhibition while multiply substituted phenyl ring of **CT-A24** hamper such favourable activity. All studied benzoxanthenes showed a very strong inhibitory effect against *S. enterica* Typhimurium TA100 cells with a survival of less than 10%. Such a drastic effect had proven that the first and major obstacle to the antibacterial action of benzoxanthenes on Gram-negative bacteria is their cell wall.

Results on *S. aureus* revealed moderate to strong antibacterial effect (growth inhibition between 60 and 90%) of BXLs (Figure 7C). **CT-A19**, **CT-A22** and especially **CT-A1** and **CT-A2** (bacteria survival < 10%) significantly inhibited the growth of *S. aureus.* This result suggests that the presence of unsubstituted or low substituted phenyl on C-1 and C-2 positions is important for such activity.

CT-A1 has no phenyl-including pendants like **CT-A2** and other **CT-A2** analogues and is structurally very similar to rufescidride which was found to be active against *S. aureus* as well.[9, 27]

Low growth inhibition on Gram-negative bacteria especially *E.coli* of the majority of studied benzoxanthenes could be ascribed to the hydrophobic nature of benzoxanthene core that hampers entering the specific cell wall structure. *S. aureus* is a Gram-positive bacterium that does not contain the outer lipopolysaccharide layer in the walls like Gram-negative bacteria.[54] Although Gram-positive bacteria contain a thicker peptidoglycan layer, they are still much more susceptible to the action of large hydrophobic compounds.

2.6. Antiproliferative activity

The antiproliferative effects of benzoxanthenes were tested *in vitro* against tumor cell lines, cervix adenocarcinoma (HeLa), colon adenocarcinoma (CaCo-2), acute lymphoblastic leukemia-derived cell line (CCRF-CEM). According to the obtained results summarized in Table 4, investigated compounds demonstrated moderate to very good inhibitory activity with IC_{50} ranging from 1 to 80 µM on human tumor cells. Nevertheless, **CT-A2** caused the highest antiproliferative effect among all studied benzoxanthenes (Table 4). This compound exhibited the same cytotoxicity as the model drug doxorubicin against HeLa tumor cell line.

These results agree with the moderate and high antiproliferative activity of **CT-A1** and **CT-A2,** respectively from previous studies on tested tumor cell lines.[13] In addition, **CT-A2** was found to be more effective in inhibiting the growth of intestinal and lung tumor cells than 5-fluorouracil.[14] For **CT-A19** and **CT-A24** the least susceptible cell line was Caco-2 (Table 4).

It can be noted that **CT-A2** showed higher activity compared to its analogues. It seems that the presence of methyl linker, but most importantly the presence of substituents on phenyl ring diminishes antiproliferative activity.

Table 4. The sensitivity of human tumor and normal cells to investigated compounds and standard anticancer drug doxorubicin.

Compound	**IC_{50} (μM)**		
	HeLa	**CaCo-2**	**CCRF-CEM**
CT-A1	18.0 ± 0.2	10.1 ± 0.4	14.1 ± 1.6
CT-A2	2.6 ± 0.9	2.9 ± 0.7	1.0 ± 0.1
CT-A4	6.3 ± 0.5	4.2 ± 1.0	8.2 ± 1.2
CT-A1	16.7 ± 0.8	10.1 ± 0.4	21.0 ± 0.9
CT-A19	6.6 ± 1.1	80.0 ± 1.1	32.4 ± 6.1
CT-A22	3.9 ± 0.0	4.4 ± 0.8	17.7 ± 0.3
CT-A23	12.1 ± 0.3	10.7 ± 0.2	14.3 ± 1.2
CT-A24	4.7 ± 1.3	74.0 ± 4.3	7.0 ± 1.3
Doxorubicin	4.2 ± 0.3	0.7 ± 0.1	0.4 ± 0.0

IC_{50} – Drug concentration that inhibited cell growth by 50%. Data represent mean IC_{50} (μM) values ± standard deviation (SD) of three independent experiments. Cytotoxicity was analyzed after 72 h of incubation using the MTT survival assay. The percentage of treated cells growth inhibition was calculated relative to the growth of untreated (control) cells.

2.7. Uptake and intracellular distribution of compound **CT-A1**

Intense fluorescence of compound **CT-A1**, when bound to DNA or RNA, allowed monitoring of their uptake and distribution in living cells by fluorescence microscopy. The uptake and intracellular distribution of compound CT-A1 were tested in the live HeLa cells after 60 or 120 minutes of incubation. During both tested periods, compound penetrated the cells and their stabile green fluorescence was scattered through the cytoplasm (Figure 8). Control, untreated cells excluded the presence of foreign fluorescence.

In comparison to DAPI which enters very fast into cells and bound primary to nuclear DNA (SI), the tested compound was spread and visible all over the treated cells. Further, more complex bioimaging has to be performed to elucidate the origin of the strong fluorescence signal of the biomacromolecule bound **CT-A1** in the cytoplasm, however that exceeds the scope of this study.[55]

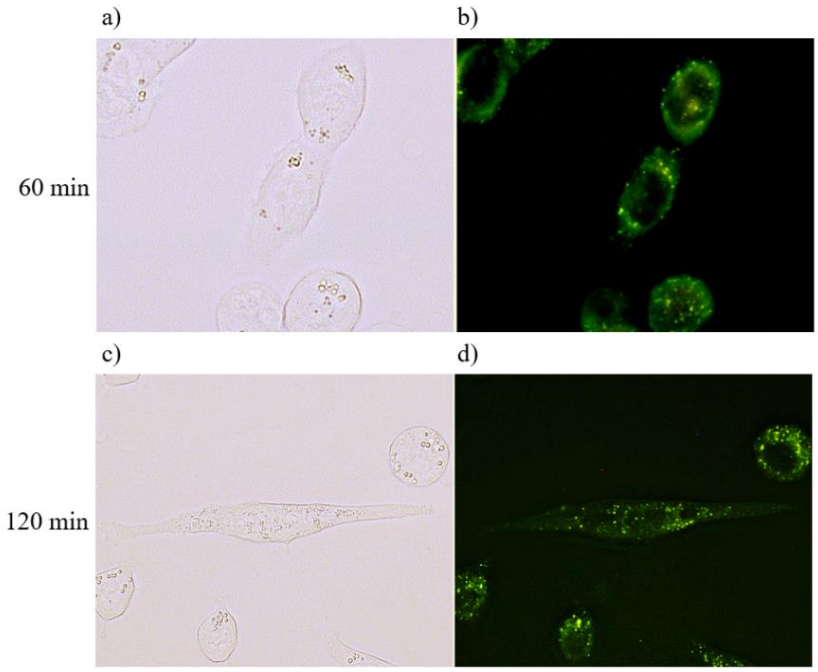

Figure 8. HeLa cells stained with 10 μM compound **CT-A1** for 60 and 120 min and analyzed under (a) visible light microscopy; (b) at λ_{exc} = 450–490 nm, λ_{em} = 520, the green fluorescence of **CT-A1**. Magnification 400 x.

2.8. Free radical scavenging activity of BXLs

The imbalance between excessive production of ROS and their immediate neutralization by the antioxidative system can lead to the disintegration of membrane lipids and damage to membrane proteins and nucleic acids. Such injury of cellular components often results in aging and contributes to the development of many human diseases including cancer.[56, 57] In this study, the commonly accepted assays DPPH and ABTS were used for the evaluation of the total antioxidant activity of benzoxanthene compounds (Figure 9). In general, all BXLs (except **CT-A14**) showed moderate to strong antiradical activity, especially with DPPH assay. **CT-A1** and **CT-A14** compounds recorded the highest and the lowest antiradical scavenging capacity, measured by either DPPH or ABTS assay, compared to other compounds. Since **CT-A1** and **CT-A14** differ only in one type of substituent at C-6, C-9 and C-10 positions of benzoxanthene ring (–OH vs –OCH3), it is evident that the extremely low antioxidant activity of **CT-A14** is due to the presence of the methoxy instead hydroxy groups on these positions. The antioxidant activity of phenolic compounds has long since been related to the presence and number of hydroxy groups, and to double bond conjugation and resonance effects.[58] Several studies found that electron-donating hydroxy substituents on the aromatic ring lower the O–H bond dissociation enthalpies (BDE) value thus enhancing the antiradical activity. Such activity is stronger for rings with pyrogallol- and catechol-like than phenol-like groups; former groups can produce highly reactive hydroxyquinone intermediates [59, 60] and can form intramolecular hydrogen bonds as well as the intermolecular hydrogen bonds with polar solvents.[59]. A good agreement between DPPH and ABTS assays was also observed for **CT-A2, CT-A4** and **CT-A23**. However, the latter two benzoxanthenes exhibited better antiradical activity than **CT-A2**. Thus, it seems that butyl linkers at C-1 and C-2 positions (**CT-A4**) cause less steric hindrance for either DPPH or ABTS radical than ethyl linkers with unsubstituted phenyl ring on those positions (**CT-A2**). The discrepancy between the two methods can be seen for **CT-A19, CT-A22** and **CT-A24**, which all displayed at least two times stronger antioxidative activity in DPPH compared to ABTS radical. The reason for that might lie in shorter (methyl) linkers at C-1

and C-2 positions of those **CT-A2** analogues, which present greater steric hindrance for ABTS radical. It is interesting that **CT-A22** exerted higher antioxidant activity in DPPH assay compared not only to **CT-A19** and **CT-A24**, but also to **CT-A2, CT-A4** and **CT-A23**. Such a result could possibly be explained as a compromise between the number of methoxy/hydroxy groups on phenyl ring and pendant alkyl linkers at C-1 and C-2 positions.

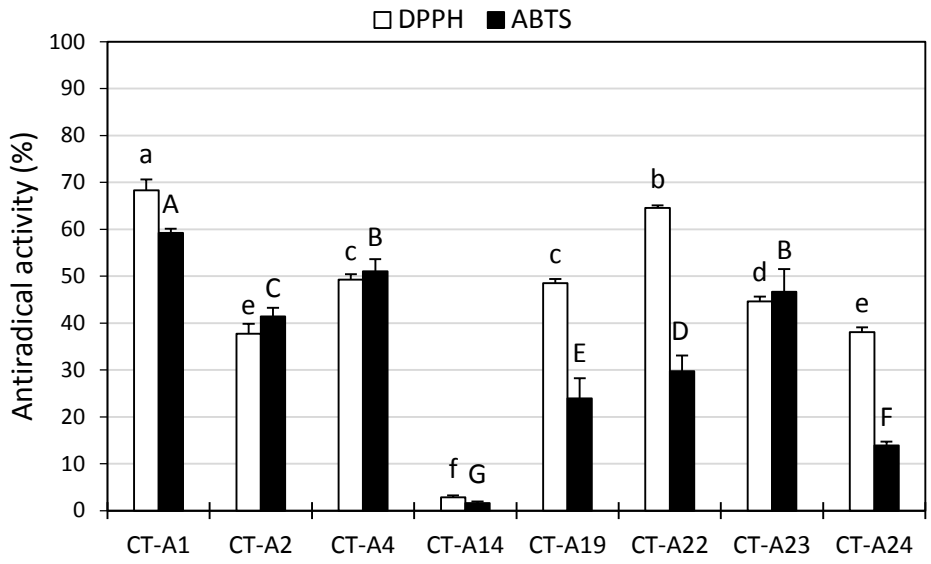

Figure 9. Antiradical activity (%) of benzoxanthene compounds using DPPH and ABTS radicals. Trolox was used as a standard antioxidant and reached 99.96 and 99.06 % antioxidant activity using DPPH and ABTS, respectively. Standard deviations are presented by error bars. Different letters indicate significantly different values at $P < 0.05$ according to ANOVA.

3. Conclusion

Until recently, there were only a few studies concerning the biological activity and possible mechanisms of action of benzoxanthenes mostly due to inefficient synthetic methods. Owing to the simple biomimetic methodology proposed by Tringali's group, this class of compounds became more available. Since the benzoxanthene **CT-A2** showed, among else, prospective antiproliferative activity and DNA damaging property in addition to the highest predicted binding affinity toward poly(dGdC)$_2$, Tringali's group prepared a small series of **CT-A2** analogues varying either in pendant alkyl linker at C-1 and C-2 (methyl or ethyl) and/or presence of methoxy/hydroxy groups on the phenyl ring.[13, 17] Besides, we included in the present study benzoxanthenes without phenyl ring at C-1 and C-2 side chains (**CT-A1**, **CT-A4** and **CT-A14**) not only for comparison reasons but because their interactions with DNA were in the previous study evaluated only with a poly(dGdC)$_2$ as a binding model.[14]

Summarized results of DNA/RNA study with BXLs (weak negative ICD spectra, moderate to high binding affinities, negligible stabilization effects of DNA and RNA) suggest a mixed binding mode, a groove binding and/or the partial intercalation. These results agree with previously published STD-NMR analysis (BMI values) obtained for **CT-A1**, **CT-A2** and **CT-A4**.[14] A study with Tel 22 revealed big stabilization effects of G-quadruplex displayed especially by **CT-A2** and **CT-A19** and weaker binding affinities of **CT-A23** and **CT-A24**. Observed 1:1 BXL-Tel22 binding stoichiometry and negligible changes in CD spectra of Tel22 suggests π-π stacking with the top or bottom quartet as the dominant interaction of benzoxanthenes. Considering the results with

ds-polynucleotides and G-quadruplex, it is noticeable that **CT-A23** and **CT-A24** bind weaker to those targets compared to other analogues, which is probably caused by steric hindrance of multiple hydroxy/methoxy substituents on the phenyl ring.

Almost all benzoxanthenes showed micromolar binding affinities toward HSA and increased protein thermal stability. Knowledge of ligand binding to HSA is useful information for all biologically active compounds because HSA affects ligand distribution *in vivo*.

Regarding free radical scavenging activity, all compounds (except **CT-A14**) displayed moderate to strong antioxidative activity with DPPH and ABTS assays, which could be related to the presence of hydroxy groups at C-6, C-9 and C-10 positions of the benzoxanthene core. After minor structural changes, **CT-A1** and **CT-A2**, in addition to **CT-A19** and **CT-A22** may be promising lead compounds for the development of new antibiotics against *S.aureus*. All examined compounds showed moderate to strong antiproliferative effects on human tumor cell lines. Despite the small differences in antiproliferative effects, **CT-A2** was shown as the most active compound on all treated tumor cells.

Our results imply that double-stranded nucleic acid structures could be one of the possible cell targets of benzoxanthenes, and this may be the basis of their antiproliferative[17] activity, and possibly antibacterial. Further tuning of benzoxantene structural features, particularly BXLs with unsubstituted phenyl ring or without phenyl ring linked to carboxyl ester groups at C-1 and C-2 appendages, could improve selectivity to ds-DNA/RNA and also preferably acquire G-quadruplex over ds-DNA selectivity. This could be primarily achieved by incorporation of positive charges, i.e. cationic side chains at C-1 and C-2 positions that could interact with DNA grooves and the negatively charged phosphate backbones of both double-stranded and G-quadruplex structures. Also, such a change in structure could further improve activity to *S. aureus* (electrostatic interactions with negatively charged teichoic acids in the cell wall) [54] but more importantly to Gram-negative bacteria.

4. Materials and Methods:

4.1. Materials and spectrophotometric methods

NMR spectra were run on a Varian Unity Inova spectrometer (Milan, Italy) operating at 499.86 (^{1}H) and 125.70 MHz (^{13}C). Chemical shifts (δ, ppm) were referenced to TMS using the residual solvent signal of acetone-d_6 (2.05 ppm). All NMR experiments, including 2D spectra, were performed using software supplied by the manufacturer and acquired at a constant temperature (300 K).

High-resolution mass spectra were acquired with an Orbitrap Fusion Tribrid®(Q-OT-qIT) mass spectrometer (Thermo Fisher Scientific, Bremen, Germany) equipped with an ESI ion source operating in positive or negative mode. Samples were directly infused and converted to the gas phase using the following parameters: source voltage, 2.6 kV; sheath gas flow rate, 25 au; and auxiliary gas, 8 au. The ions were introduced into the mass spectrometer through a heated ion transfer tube (300 °C). A survey scan was performed from m/z 150 to 1000 at 500k resolution (@ 200 m/z) using the following parameters: RF lens, 60%; auto gain control target, 20,000.

Caffeic acid, caffeic acid phenethyl ester (**2b**), MeI, $Mn(OAc)_3$ and the alcohols employed in the esterification were purchased from Sigma Aldrich. *N,N'*-dicyclohexylcarbodiimide (DCC) was purchased from TCI.

The UV/vis spectra were recorded on a Varian Cary 100 Bio spectrophotometer, CD spectra on JASCO J815 spectrophotometer and fluorescence spectra on a Varian Cary Eclipse spectrophotometer at 25 °C using appropriate 1cm path quartz cuvettes.

Polynucleotides were purchased as noted: poly A–poly U, poly(dAdT)$_2$, poly(dGdC)$_2$ and calf thymus ctDNA (Sigma-Aldrich). Polynucleotides were dissolved in Na-cacodylate buffer, *I*=0.05 mol dm^{-3}, pH=7. The calf thymus ctDNA was additionally sonicated and filtered through a 0.45 mm filter.[61] Polynucleotide concentration was determined spectroscopically[62, 63] as the concentration of phosphates. Spectrophotometric titrations were performed at pH=7 (*I*=0.05 mol dm^{-3}, sodium cacodylate buffer) by adding portions of the polynucleotide solution into the solution of the studied compound for fluorimetric experiments and CD experiments were done by adding portions of the compound stock solution into the solution of a polynucleotide. In fluorimetric experiments excitation wavelengths of λ_{exc}=302 and 393-400 nm were used to avoid the inner filter effect caused due to increasing absorbance of the polynucleotide. Emission was collected in the range λ_{em}=450–650 nm. Values for K_s obtained by processing titration data using the Scatchard equation (Tables 1 and 3), all have satisfactory correlation coefficients (>0.99). Thermal melting curves for DNA, RNA and their complexes with studied compounds were determined as previously described by following the absorption change around 260 nm as a function of temperature. The absorbance of the ligands was subtracted from every curve, and the absorbance scale was normalized. T_m values are the midpoints of the transition curves determined from the maximum of the first derivative and checked graphically by the tangent method. The ΔT_m values were calculated subtracting T_m of the free nucleic acid from T_m of the complex. Every ΔT_m value here reported was the average of at least two measurements. The error in ΔT_m is ±0.5ºC. 5'- AGGG(TTAGGG)3–3' (Tel22) was obtained from IDT (Integrated DNA Technologies), USA. Tel22 was dissolved in 0.1 M sodium cacodylate buffer. The starting Tel22 oligonucleotide solution was first heated up to 95 °C for 10 minutes and then slowly cooled to 10 °C at the cooling rate of 1 °C/ min to allow DNA oligonucleotide to adopt G-quadruplex structure.[64] The G-quadruplex structure was confirmed by thermal melting and CD spectra.[65, 66] The concentration of G-quadruplex was expressed in terms of oligonucleotide structure for calculations of stability constants from fluorimetric titrations. For thermal melting experiments and CD titrations, the concentration of G-quadruplex was expressed in terms of a monomeric unit (G-quartet). In fluorimetric titrations, aliquots of Tel 22 solution were added to the solution of BXLs (c=2-3×10^{-6} M). Human serum albumin was purchased from Sigma-Aldrich and dissolved in 0.05 M sodium cacodylate buffer.

4.2. Synthesis of benzoxanthene lignans

Caffeoyl esters **2a** and **2c** were obtained by treating caffeic acid with methanol or butyl alcohol as previously reported.[14] The esters **2d**-**g** were obtained by Steglich reaction, as previously described.[18] Briefly, caffeic acid (500 mg, 2.7 mmol) was solubilized in dry THF (20 mL) and treated with DCC (1.2 equiv) under stirring at 70 °C for 10 min. The proper alcohol was added and the mixture was refluxed for 8 h. The mixture was filtered off and the crude was purified by column chromatography on diol silica gel. The spectral data of esters **2d**-**g** were in agreement with those previously reported.[67]

Benzoxanthene lignans were obtained as previously reported[67]: each ester **2a**-**g** (1.0 mmol) was treated with a suspension of Mn(OAc$_3$) in $CHCl_3$ (4.0 mmol in 50 mL). The mixture was stirred at rt for 3 h. The reaction was quenched with a saturated ascorbic acid solution and the two phases were recovered. The aqueous layer was partitioned with CH_2Cl_2 (three times) and the combined organic phase was dried over Na_2SO_4 anhydrous, filtered and took to dry. The proper benzoxanthene was recovered from the organic phase by column chromatography on Diol silica gel. The spectral data of **CT-A1**, **CT-A2**, **CT-A4**, **CT-A19**, **CT-A22** were in agreement with those previously reported.[13, 14, 18]

Compound **CT-A23** was obtained with 38.8%. ^{1}H NMR (500 MHz, acetone-d_6) δ 8.11 (s, 1H, H-3), 7.47 (d, *J* = 8.7 Hz, 1H, H-4), 7.32 (*J* = 8.7 Hz, 1H, H-5), 7.28 (s, 1H, H-11), 6.96 (bs, 1H, H-2'''), 6.89 (bs, 1H, H-2''), 6.78 (s, 2H, H-8 and H-6'''), 6.74 (bs, 1H,

H-6''), 6.73 (bs, 1H, H-5''), 6.71 (bs 1H, H-5'''), 4.57 (t, *J* = 7.0 Hz, 2H, C*H*$_2$-8''), 4.40 (t, *J* = 7.0 Hz, 2H, C*H*$_2$-8'''), 3.81 (s, 3H, OC*H*$_3$), 3.76 (s, 3H, OC*H*$_3$), 3.00 (m, 4H, C*H*$_2$-7'' and C*H*$_2$-7'''. ^{13}C NMR (125 MHz, acetone-d_6) δ 170.7 (C, C-1'), 166.6 (C, C-2'), 149.1 (C, C-9), 148.3 (C, C-3'''), 148.2 (C, C-3''), 147.8 (C, C-10), 146.2 (C, C-4'''), 146.1 (C, C-4''), 142.8 (C, C-6), 142.6 (C, C-6a), 137.7 (C, C-7), 130.2 (C, C-1'''), 130.1 (C, C-1''), 129.6 (CH, C-3), 127.6 (C, C-3a), 126.2 (CH, C-4), 125.1 (C, C-11b), 124.2 (C, C-11c), 122.4 (CH, C-6'''), 122.2 (C, C-2 and CH, C-6''), 122.1 (C, C-1), 120.7 (CH, C-5), 115.8 (CH, C-5'''), 115.7 (CH, C-5''), 113.5 (CH, H-2''), 113.4 (CH, H-2'''), 112.4 (CH, C-11), 111.0 (C, C-11a), 104.8 (CH, C-8), 67.1 (CH_2, C-8''), 66.9 (CH_2, C-8'''), 56.2 (CH_3, O*C*H$_3$), 56.1 (CH_3, OC*H*$_3$), 35.3 (CH_2, C-7'''), 34.8 (CH_2, C-7'''). HRESIMS *m/z* 653.1682 $[M-H]^-$ (calcd for $C_{36}H_{29}O_{12}$: 653.1659).

Compound **CT-A24** was obtained with 35.4%. ^{1}H NMR (500 MHz, acetone-d_6) δ 8.19 (s, 1H, H-3), 7.52 (d, *J* = 9.5 Hz, 1H, H-4), 7.33 (s, 1H, H-11), 7.31 (*J* = 9.5 Hz, 1H, H-5), 6.72 (s, 1H, H-8), 6.84 (s, 2H, H-2'''/H-6'''), 6.64 (s 2H, H-2''/H-6''), 5.26 (s, 2H, H-7'''), 5.15 (s, 2H, H-7''), 3.85 (s, 6H, OC*H*$_3$ at C-3'''/C-5'''), 3.74 (s, 6H, OC*H*$_3$ at C-3''/C-5''), 3.73 (s, 3H, OC*H*$_3$ at C-4'''), 3.67 (s, 3H, OC*H*$_3$ at C-4''). ^{13}C NMR (125 MHz, acetone-d_6) δ 172.5 (C, C-1'), 168.6 (C, C-2'), 156.2 (C, C-3'''/C-5'''), 156.1 (C, C-3''/C-5''), 150.8 (C, C-9), 149.6 (C, C-10), 144.5 (C, C-6), 144.3 (C, C-7a), 141.0 (C, C-4'''), 140.8 (C, C-4''), 139.3 (C, C-6a), 134.0 (C, C-1'''), 133.5 (C, C-1''), 131.6 (CH, C-3), 129.3 (C, C-3a), 128.0 (C, C-2), 127.0 (C, C-11b), 125.9 (C, C-11c), 124.0 (CH, C-4), 123.2 (C, C-1), 122.4 (CH, C-5), 114.0 (CH, C-11), 112.7 (C, C-11a), 108.7 (CH, C-2'''/C-6'''), 108.6 (CH, C-2''/C-6''), 106.5 (CH, H-8), 70.2 (CH_2, C-7''), 69.8 (CH_2, C-7'''), 62.3 (CH_3, 4'''-OCH_3), 62.1 (CH_3, 4''-OCH_3), 58.2 (CH_3, 3'''/5'''-OCH_3), 58.0 (CH_3, 3''/5''-OCH_3). HRESIMS *m/z* 713.1829 $[M-H]^-$ (calcd for $C_{38}H_{33}O_{14}$: 713.1870).

Compound **CT-A14** was obtained as previously reported.[13]

4.3. Differential scanning calorimetry (DSC)

Changes in the thermostability of HSA in the absence and presence of studied benzoxanthene compounds were monitored using DSC. DSC analyses of HSA solutions and benzoxanthene-HSA complexes were done using TA Instruments Nano DSC device. All solutions were degassed before measurement for 15 min each. Measurements were carried out over temperature range 20-95 °C following equilibration for 10 min at 20 °C. The temperature scan rate was 1 °C/min. The cell volume was 0.3 mL. The concentration of HSA was 2 x 10^{-5} M for all measurements, while concentrations of benzoxanthene compounds varied (4×10^{-5} M – 1.2×10^{-4} M), resulting with ***r*** values ([compound]/ [HSA]) = 1-4. Values ***r*** [compound]/ [HSA] for each complex were chosen according to results of fluorimetric titrations. DSC curves were analyzed with TA NanoAnalyse software. Buffer scan was subtracted from every thermogram, while calorimetric data were also corrected for the difference in heat capacity between the initial and the final state by using a sigmoidal baseline. The results were shown in the form of heat capacity at constant pressure (Cp, p= 3 atm) *vs* temperature curves (DSC thermograms, SI).

4.4. Cytotoxic effect of benzoxantane lignans

Bacterial strains used in this work are a part of microorganism collection kept and maintained in Laboratory for biology and microbial genetics, Faculty of food technology and biotechnology, Zagreb. All strains were deposited at -80 ˚C in liquid media and the presence of 10 % glycerol. Before experiments, 100 µL of bacterial strain was inoculated into 20 mL of fresh medium and grown at optimal growth temperature to an exponential growth phase.

Cytotoxic effect of benzoxantane lignans was determined on *E. coli* K-12 MG1655*, S. enterica* serovar Typhimurium LT21*, S. enterica* serotip Typhimurium TA100*, S. aureus.*

Briefly, 20 µL of cell suspension grown to the exponential phase was seeded in microtiter plates. Cells were treated with 20 µL of the examined compound at the final concentration of 50 µM. As a negative control, phosphate buffer was added instead of benzoxantane lignans. Cells were treated for 1 h. Afterward, microdilutions of preincubation mixtures were prepared and cells were seeded onto agar plates. After 24 h of incubation at 37 °C, the number of grown cells was counted, compared to negative control and the percentage of cell survival was counted. Each compound was tested in triplicate and experiments were repeated three times.

4.5. Antiproliferative effect of benzoxantane lignans

Antiproliferative effect of tested compounds was carried out on cervix adenocarcinoma (HeLa), colon adenocarcinoma (CaCo-2), acute lymphoblastic leukemia-derived cell line (CCRF-CEM). Adherent cells were cultured in DMEM supplemented with 10% heat-inactivated FBS and 2 mM glutamine. Cells in suspension were grown in RPMI 1640 medium supplemented with 10% FBS, 2 mM glutamine, 10 mM sodium pyruvate and 2 mM HEPES. The cells were grown as monolayers or suspensions in tissue culture flasks (BD Falcon, Germany) in the humidified atmosphere under the conditions of 37°C/5% of CO_2 gas in the CO_2 incubator (IGO 150 CELLlife™, JOUAN, ThermoFisher Scientific, Waltham, MA, USA). Cells growth was determined using the colorimetric methyltetrazolium (MTT) assay after 72 h of the exposure tested derivatives. The cells were seeded in 96 micro-well plates at a concentration of 2×10^4 cells/mL for adherent cells and $1x10^5$ cells/mL for leukemia and lymphoma cells.

Doxorubicin was used as a model compound. It was dissolved in highly pure water as a stock solution at 10 mM. Tested compounds were prepared as stock solutions (10 mM) in dimethylsulfoxide (DMSO). Working solutions (100 – 0.1 µM) were prepared in the cell culture medium. Effect of solvent (DMSO) on cell growth was also tested by adjusting concentration range to be the same as in working concentrations of tested compounds were applied in concentrations of 100, 10 and 1 µM during 72 h. After the expired time of incubation, 5 mg/mL MTT solution was added to each well and incubated for 4 h in the CO_2 incubator. Formazane crystals were dissolved in DMSO or 10% SDS with 0.01 M HCl and absorbance was measured at 595 nm on a microplate reader (iMark, BIO-RAD, Hercules, CA, USA). Control (non-treated) cells were grown under the same conditions. All experiments were performed at least three times in triplicates.

The percentage of cell growth (PG) was calculated using the following equation:

$PG = (A_{compound} – A_{background} / A_{control} – A_{background})$ x100, where $A_{background}$ is the absorbance of MTT solution and DMSO; and $A_{control}$ is the absorbance of cells' suspension grown without tested compounds.

The IC_{50} value, defined as a compound concentration leading to cellular viability reduction by 50%, was calculated and used as a comparison parameter. The calculation of IC_{50} values curves is performed by using Excel tools. Briefly, individual concentration-effect curves are generated by plotting the logarithm of the concentration of tested compounds.

4.6. Fluorescence microscopy

HeLa cells were grown on microscopic slides/glass coverslip (1×10^5 cells/mL) at 37°C for 24 h in a humidified atmosphere with 5% CO_2. Compound CT-A1 stock solution (c = 500 µM) was diluted to the final concentration (c = 10 µM) in DME medium before

the test. 4′,6-Diamidino-2-phenylindole dihydrochloride (DAPI) methanol solution (1 nM) was applied as a dye for nucleus staining in the same manner as a tested compound. Cells were incubated with 10 μM compound CT-A1 (in DMEM medium) for 30, 60 and 120 min, washed with PBS and analyzed. To confirm the viability of the cells, control cells were treated in propidium iodide (PI) solution (0.01 μM) for 60 min, washed with PBS and analyzed under a microscope (PBS as mounting medium). The entry and intracellular distribution of tested compound were analyzed under the fluorescence microscope (Axioscope 2 MOT, Carl Zeiss Jena GmbH, Jena, Germany) with Zeiss filter combinations: (f3) BP 450-495, LP 525 for 1 and 2; (f1) BP 365/12, FT 395, LP 397 for DAPI; and (f2) BP 530 – 585, FT 600, LP 615 for PI. Untreated cells as negative control exclude the presence of foreign fluorescence.

4.7. Antiradical activity

BXLs were dissolved in DMSO to a concentration of 2 mM. The total antioxidant capacity of BXLs was assessed in their final concentration of 0.01 mM using a stable free radical 1,1-diphenyl-2-picrylhydrazyl (DPPH) or 2,2-azino-bis(3-ethylbenzothiazoline-6-sulphonic acid (ABTS). In both assays, Trolox (dissolved in DMSO) was used as a standard antioxidant compound in the same final concentration (0.01 mM) as BXLs. The DPPH assay was performed following the method of Germano et al.[68] with slight modifications. Briefly, 0.01 ml of each BXL or Trolox was added to freshly prepared 0.1 mM methanolic DPPH solution (final volume 2 ml) and incubated in the dark for 30 min at 25 °C. The absorbance was measured at 515 nm.

The radical scavenging activities were calculated according to the equation: % inhibition = (A0 - At/A0) × 100, where A0 is the absorbance of the control (blank, without either BXLs or Trolox) and At is the absorbance in the presence of either BXLs or Trolox. The ABTS assay was carried out according to Re et al.[69] Each BXL or Trolox (0.01 ml) was added to ABTS solution (final volume 2 ml), incubated for 30 min at 25 °C and absorbance was read at 734 nm. The radical scavenging capacity was calculated as a percent of DPPH inhibition, according to the equation described above. All absorbance measurements were performed on a spectrophotometer (Analytik Jena Specord 40, Analytik Jena, Upland, CA, USA).

4.8. Statistical analysis

Results for antioxidative activity were evaluated using the software package Statistica 13.3 (TIBCO Software Inc., United States). Results were subjected to one-way ANOVA for comparison of means and significant differences were calculated according to Duncan's multiple range test. Data were considered statistically significant at $P < 0.05$. Different letters indicate significant difference at $P < 0.05$.

Acknowledgments:

Financial support from the Croatian Science Foundation under the project IP-2018-01-4694, Croatian Academy of Sciences and Arts and from MIUR ITALY PRIN 2017 (Project No. 2017A95NCJ) is gratefully acknowledged.

Author Contributions

The manuscript was written through the contributions of all authors. All authors have approved the final version of the manuscript.

Declarations of interest: none.

References:

[1] F. Zalesak, D.J.Y.D. Bon, J. Pospisil, Lignans and Neolignans: Plant secondary metabolites as a reservoir of biologically active substances, Pharmacol Res 146(104284) (2019) 1-27.
[2] D.C. Ayres, J.D. Loike, Lignans : chemical, biological, and clinical properties, Cambridge University Press, Cambridge, 1990.
[3] S. Apers, Vlietinck, A., Pieters, L. , Lignans and neolignans as lead compounds, Phytochemistry Reviews 2 (2003) 201-217.
[4] A.K. Prasad, V. Kumar, P. Arya, S. Kumar, R. Dabur, N. Singh, A.K. Chhillar, G.L. Sharma, B. Ghosh, J. Wengel, C.E. Olsen, V.S. Parmar, Investigations toward new lead compounds from medicinally important plants, Pure Appl Chem 77(1) (2005) 25-40.
[5] S. Apers, D. Paper, J. Burgermeister, S. Baronikova, S. Van Dyck, G. Lemiere, A. Vlietinck, L. Pieters, Antiangiogenic activity of synthetic dihydrobenzofuran lignans, J Nat Prod 65(5) (2002) 718-720.
[6] E.L. Ghisalberti, Cardiovascular activity of naturally occurring lignans, Phytomedicine 4(2) (1997) 151-166.
[7] M. Gordaliza, M.A. Castro, J.M.M. del Corral, A. San Feliciano, Antitumor properties of podophyllotoxin and related compounds, Curr Pharm Design 6(18) (2000) 1811-1839.
[8] K.R. Hande, Etoposide: four decades of development of a topoisomerase II inhibitor, Eur J Cancer 34(10) (1998) 1514-21.
[9] S.A.S. da Silva, A.L. Souto, M.D. Agra, E.V.L. da-Cunha, J.M. Barbosa, M.S. da Silva, R. Braz Filho, A new arylnaphthalene type lignan from Cordia rufescens A. DC. (Boraginaceae), Arkivoc (2004) 54-58.
[10] L.B. Davin, H.B. Wang, A.L. Crowell, D.L. Bedgar, D.M. Martin, S. Sarkanen, N.G. Lewis, Stereoselective bimolecular phenoxy radical coupling by an auxiliary (dirigent) protein without an active center, Science 275(5298) (1997) 362-6.
[11] L. Pieters, S. Van Dyck, M. Gao, R. Bai, E. Hamel, A. Vlietinck, G. Lemiere, Synthesis and biological evaluation of dihydrobenzofuran lignans and related compounds as potential antitumor agents that inhibit tubulin polymerization, J Med Chem 42(26) (1999) 5475-81.
[12] C. Daquino, A. Rescifina, C. Spatafora, C. Tringali, Biomimetic Synthesis of Natural and "Unnatural" Lignans by Oxidative Coupling of Caffeic Esters, Eur J Org Chem (36) (2009) 6289-6300.
[13] S. Di Micco, F. Mazue, C. Daquino, C. Spatafora, D. Delmas, N. Latruffe, C. Tringali, R. Riccio, G. Bifulco, Structural basis for the potential antitumour activity of DNA-interacting benzo[kl]xanthene lignans, Org Biomol Chem 9(3) (2011) 701-710.
[14] C. Spatafora, V. Barresi, V.M. Bhusainahalli, S. Di Micco, N. Musso, R. Riccio, G. Bifulco, D. Condorelli, C. Tringali, Bio-inspired benzo[k,l]xanthene lignans: synthesis, DNA-interaction and antiproliferative properties, Org Biomol Chem 12(17) (2014) 2686-2701.
[15] C. Spatafora, C. Daquino, C. Tringali, R. Amorati, Reaction of benzoxanthene lignans with peroxyl radicals in polar and non-polar media: cooperative behaviour of OH groups, Org Biomol Chem 11(26) (2013) 4291-4294.
[16] G. Basini, L. Baioni, S. Bussolati, F. Grasselli, C. Daquino, C. Spatafora, C. Tringali, Antiangiogenic properties of an unusual benzo[k,l]xanthene lignan derived from CAPE (Caffeic Acid Phenethyl Ester), Invest New Drug 30(1) (2012) 186-190.
[17] V. Vijayakurup, C. Spatafora, C. Daquino, C. Tringali, P. Srinivas, S. Gopala, Phenethyl caffeate benzo[kl]xanthene lignan with DNA interacting properties induces DNA damage and apoptosis in colon cancer cells, Life Sci 91(25-26) (2012) 1336-1344.
[18] C. Genovese, L. Pulvirenti, N. Cardullo, V. Muccilli, G. Tempera, D. Nicolosi, C. Tringali, Bioinspired benzoxanthene lignans as a new class of antimycotic agents: synthesis and Candida spp. growth inhibition, Nat Prod Res (2018) 1-10.
[19] J. Gerstmeier, C. Kretzer, S. Di Micco, L. Miek, H. Butschek, V. Cantone, R. Bilancia, R. Rizza, F. Troisi, N. Cardullo, C. Tringali, A. Ialenti, A. Rossi, G. Bifulco, O. Werz, S. Pace, Novel benzoxanthene

lignans that favorably modulate lipid mediator biosynthesis: A promising pharmacological strategy for anti-inflammatory therapy, Biochem Pharmacol 165 (2019) 263-274.
[20] A. Capolupo, A. Tosco, M. Mozzicafreddo, C. Tringali, N. Cardullo, M.C. Monti, A. Casapullo, Proteasome as a New Target for Bio-Inspired Benzo[k,l]xanthene Lignans, Chem-Eur J 23(35) (2017) 8371-8374.
[21] B. Aslam, W. Wang, M.I. Arshad, M. Khurshid, S. Muzammil, M.H. Rasool, M.A. Nisar, R.F. Alvi, M.A. Aslam, M.U. Qamar, M.K.F. Salamat, Z. Baloch, Antibiotic resistance: a rundown of a global crisis, Infect Drug Resist 11 (2018) 1645-1658.
[22] M. Maruyama, S. Yamauchi, K. Akiyama, T. Sugahara, T. Kishida, Y. Koba, Antibacterial activity of a virgatusin-related compound, Bioscience, biotechnology, and biochemistry 71(3) (2007) 677-80.
[23] C.B. M. Demeunynck, W.D. Wilson, DNA and RNA Binders, Wiley-VCH, Weinheim, 2002.
[24] S. Neidle, Oxford Handbook of Nucleic Acid Structure, 1 edition ed., Oxford University Press, Oxford, 1999.
[25] C.R. Cantor, P.R. Schimmel, Biophysical Chemistry, W.H. Freeman and Co., San Francisco, 1980.
[26] S. Bhaduri, N. Ranjan, D.P. Arya, An overview of recent advances in duplex DNA recognition by small molecules, Beilstein J Org Chem 14 (2018) 1051-1086.
[27] X. Li, S. Shi, Y. Xu, Q. Tao, J. Stockhit, Y. Zhao, Lignin in dandelion, its bacteria-resisting activity and use for medicine, CN Pat 101024640 (2007).
[28] W. Saenger, Principles of nucleic acid structure, Springer-Verlag New York, New York, 1984.
[29] G. Scatchard, The attractions of proteins for small molecules and ions, Annals of the New York Academy of Sciences 51(4) (1949) 660-672.
[30] J.D. Mcghee, Correction, J Mol Biol 103(3) (1976) 679-679.
[31] J.L. Mergny, L. Lacroix, Analysis of thermal melting curves, Oligonucleotides 13(6) (2003) 515-37.
[32] A. Rodger, B. Norden, Circular Dichroism and Linear Dichroism, Oxford University Press, Oxford, 1997.
[33] N. Berova, K. Nakanishi, R.W. Woody, Circular dichroism Principles and Applications, 2nd Edition, Wiley-VCH, New York, 2000.
[34] M. Eriksson, B. Norden, Linear and circular dichroism of drug-nucleic acid complexes, Method Enzymol 340 (2001) 68-98.
[35] T. Smidlehner, I. Piantanida, G. Pescitelli, Polarization spectroscopy methods in the determination of interactions of small molecules with nucleic acids - tutorial, Beilstein J Org Chem 14 (2018) 84-105.
[36] S. Di Micco, C. Bassarello, G. Bifulco, R. Riccio, L. Gomez-Paloma, Differential-frequency saturation transfer difference NMR spectroscopy allows the detection of different ligand-DNA binding modes, Angew Chem Int Edit 45(2) (2006) 224-228.
[37] S.L. Cree, M.A. Kennedy, Relevance of G-quadruplex structures to pharmacogenetics, Front Pharmacol 5 (2014).
[38] M.L. Bochman, K. Paeschke, V.A. Zakian, DNA secondary structures: stability and function of G-quadruplex structures, Nat Rev Genet 13(11) (2012) 770-80.
[39] M.C. Miller, R. Buscaglia, J.B. Chaires, A.N. Lane, J.O. Trent, Hydration is a major determinant of the G-quadruplex stability and conformation of the human telomere 3' sequence of d(AG3(TTAG3)3), J Am Chem Soc 132(48) (2010) 17105-7.
[40] Y. Wang, D.J. Patel, Solution structure of the human telomeric repeat d[AG3(T2AG3)3] G-tetraplex, Structure 1(4) (1993) 263-82.
[41] H. Gampp, M. Maeder, C.J. Meyer, A.D. Zuberbuhler, Calculation of equilibrium constants from multiwavelength spectroscopic data--II: SPECFIT: two user-friendly programs in basic and standard FORTRAN 77, Talanta 32(4) (1985) 257-64.
[42] C.I.V. Ramos, S.P. Almeida, L.M.O. Lourenco, P.M.R. Pereira, R. Fernandes, M.A.F. Faustino, J.P.C. Tome, J. Carvalho, C. Cruz, M. Neves, Multicharged Phthalocyanines as Selective Ligands for G-Quadruplex DNA Structures, Molecules 24(4) (2019).
[43] M. Maciazek-Jurczyk, A. Szkudlarek, M. Chudzik, J. Pozycka, A. Sulkowska, Alteration of human serum albumin binding properties induced by modifications: A review, Spectrochim Acta A Mol Biomol Spectrosc 188 (2018) 675-683.

[44] G. Sudlow, D.J. Birkett, D.N. Wade, Characterization of 2 Specific Drug Binding-Sites on Human-Serum Albumin, Mol Pharmacol 11(6) (1975) 824-832.
[45] G. Sudlow, D.J. Birkett, D.N. Wade, Further Characterization of Specific Drug Binding-Sites on Human-Serum Albumin, Mol Pharmacol 12(6) (1976) 1052-1061.
[46] D. Buttar, N. Colclough, S. Gerhardt, P.A. MacFaul, S.D. Phillips, A. Plowright, P. Whittamore, K. Tam, K. Maskos, S. Steinbacher, H. Steuber, A combined spectroscopic and crystallographic approach to probing drug-human serum albumin interactions, Bioorganic & medicinal chemistry 18(21) (2010) 7486-96.
[47] J. Ghuman, P.A. Zunszain, I. Petitpas, A.A. Bhattacharya, M. Otagiri, S. Curry, Structural basis of the drug-binding specificity of human serum albumin, J Mol Biol 353(1) (2005) 38-52.
[48] F. Zsila, Z. Bikadi, D. Malik, P. Hari, I. Pechan, A. Berces, E. Hazai, Evaluation of drug-human serum albumin binding interactions with support vector machine aided online automated docking, Bioinformatics 27(13) (2011) 1806-13.
[49] J.L. Lahti, G.W. Tang, E. Capriotti, T.Y. Liu, R.B. Altman, Bioinformatics and variability in drug response: a protein structural perspective, J R Soc Interface 9(72) (2012) 1409-1437.
[50] A. Michnik, Michalik, K., Kluczewska, A., Drzazga, Z., Comparative DSC study of human and bovine serum albumin, Journal of Thermal Analysis and Calorimetry 84 (2006) 113–117.
[51] M.S. M. Nišavić, I. Crnolatac, M. Milošević, A. Rilak, R. Masnikosa, Highly water-soluble ruthenium(II) terpyridine coordination compounds form stable adducts with blood-borne metal transporting proteins, Arab. J. Chem. 11(3) (2018) 291-304.
[52] T.M. Nobre, M.W. Martynowycz, K. Andreev, I. Kuzmenko, H. Nikaido, D. Gidalevitz, Modification of Salmonella Lipopolysaccharides Prevents the Outer Membrane Penetration of Novobiocin, Biophys J 109(12) (2015) 2537-2545.
[53] H. Nikaido, Outer Membrane of Salmonella-Typhimurium Transmembrane Diffusion of Some Hydrophobic Substances, Biochim Biophys Acta 433(1) (1976) 118-132.
[54] L. Brown, J.M. Wolf, R. Prados-Rosales, A. Casadevall, Through the wall: extracellular vesicles in Gram-positive bacteria, mycobacteria and fungi, Nat Rev Microbiol 13(10) (2015) 620-630.
[55] R.W. Horobin, S. Trapp, V. Weissig, Mitochondriotropics: A review of their mode of action, and their applications for drug and DNA delivery to mammalian mitochondria, J Control Release 121(3) (2007) 125-136.
[56] M. Katerji, M. Filippova, P. Duerksen-Hughes, Approaches and Methods to Measure Oxidative Stress in Clinical Samples: Research Applications in the Cancer Field, Oxidative medicine and cellular longevity 2019 (2019) 1279250.
[57] I. Grigalius, V. Petrikaite, Relationship between Antioxidant and Anticancer Activity of Trihydroxyflavones, Molecules 22(12) (2017).
[58] C.A. Rice-Evans, N.J. Miller, G. Paganga, Structure-antioxidant activity relationships of flavonoids and phenolic acids, Free radical biology & medicine 20(7) (1996) 933-56.
[59] H.-Y. Zhang, Sun, Y.-M., Wang, X.-L. , Substituent effects on O–H bond dissociation enthalpies and ionization potentials of catechols: A DFT study and its implications in the rational design of phenolic antioxidants and elucidation of structure–activity relationships for flavonoid antioxidants, Chemistry – A European Journal 9(2) (2003) 502–508.
[60] R. Farhoosh, S. Johnny, M. Asnaashari, N. Molaahmadibahraseman, A. Sharif, Structure-antioxidant activity relationships of o-hydroxyl, o-methoxy, and alkyl ester derivatives of p-hydroxybenzoic acid, Food chemistry 194 (2016) 128-34.
[61] J.B. Chaires, N. Dattagupta, D.M. Crothers, Studies on Interaction of Anthracycline Antibiotics and Deoxyribonucleic-Acid - Equilibrium Binding-Studies on Interaction of Daunomycin with Deoxyribonucleic-Acid, Biochemistry-Us 21(17) (1982) 3933-3940.
[62] J.L. Bresloff, D.M. Crothers, Equilibrium Studies of Ethidium-Polynucleotide Interactions, Biochemistry-Us 20(12) (1981) 3547-3553.
[63] T.V. Chalikian, J. Volker, G.E. Plum, K.J. Breslauer, A more unified picture for the thermodynamics of nucleic acid duplex melting: A characterization by calorimetric and volumetric techniques, P Natl Acad Sci USA 96(14) (1999) 7853-7858.

[64] M. Boncina, C. Podlipnik, I. Piantanida, J. Eilmes, M.P. Teulade-Fichou, G. Vesnaver, J. Lah, Thermodynamic fingerprints of ligand binding to human telomeric G-quadruplexes, Nucleic acids research 43(21) (2015) 10376-86.
[65] M. Babinsky, R. Fiala, I. Kejnovska, K. Bednarova, R. Marek, J. Sagi, V. Sklenar, M. Vorlickova, Loss of loop adenines alters human telomere d[AG3(TTAG3)3] quadruplex folding, Nucleic acids research 42(22) (2014) 14031-41.
[66] A. Ambrus, D. Chen, J. Dai, T. Bialis, R.A. Jones, D. Yang, Human telomeric sequence forms a hybrid-type intramolecular G-quadruplex structure with mixed parallel/antiparallel strands in potassium solution, Nucleic acids research 34(9) (2006) 2723-35.
[67] J. Zhang, L.X. Xu, X.S. Xu, B.W. Li, R. Wang, J.J. Fu, Synthesis and effects of new caffeic acid derivatives on nitric oxide production in lipopolysaccharide-induced RAW 264.7 macrophages, International journal of clinical and experimental medicine 7(4) (2014) 1022-7.
[68] M.P. Germano, R. De Pasquale, V. D'Angelo, S. Catania, V. Silvari, C. Costa, Evaluation of extracts and isolated fraction from Capparis spinosa L. buds as an antioxidant source, Journal of agricultural and food chemistry 50(5) (2002) 1168-71.
[69] R. Re, N. Pellegrini, A. Proteggente, A. Pannala, M. Yang, C. Rice-Evans, Antioxidant activity applying an improved ABTS radical cation decolorization assay, Free radical biology & medicine 26(9-10) (1999) 1231-7.

Graphical abstract:

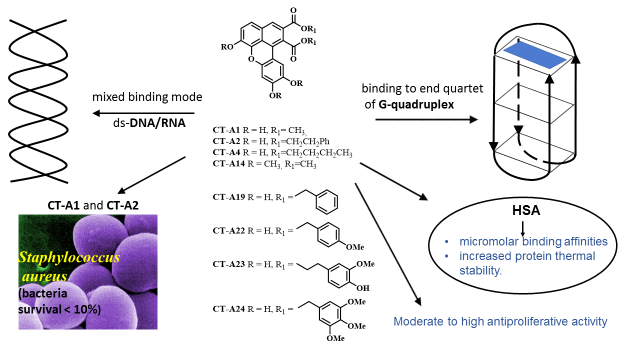

Declaration of interests

☒ The authors declare that they have no known competing financial interests or personal relationships that could have appeared to influence the work reported in this paper.

☐The authors declare the following financial interests/personal relationships which may be considered as potential competing interests: